

Automated Determination of Snow Water Equivalent by Acoustic Reflectometry

Nicholas J. Kinar and John W. Pomeroy

Abstract—Snow water equivalent (SWE) is commonly determined using gravimetric and depth measurement techniques. Previous research has demonstrated the ability to determine SWE from the propagation and reflection of acoustic waves. Despite the advantages of the acoustic technique, it has not been adapted so that SWE can be determined in an automated fashion. This paper presents a new technique for determining SWE by the application of acoustics. A maximum-length sequence was used as the input to the layered snowpack system. Signal processing of the reflected wave and a recursive algorithm was used to model the sound pressure wave as it passed through the snowpack. Embedded systems were designed to implement the signal processing and calculations so that SWE could be quickly determined at a field location. The systems were deployed at sites near Whitehorse, YT, and at sites in the Rocky Mountains of Alberta, Canada. Comparisons were made between SWE estimated by the acoustic technique and SWE determined by gravimetric sampling. These comparisons demonstrated that the acoustic SWE measurement performed with the embedded systems and the new signal processing technique can provide SWE estimates that are of comparable accuracy to SWE calculated from gravimetric samples.

Index Terms—Acoustic devices, acoustic propagation, acoustics, acoustic signal processing, snow.

I. INTRODUCTION

SNOW water equivalent (SWE) is the equivalent depth of water that would be available if the snowpack were transformed to liquid water [1]. The measurement of SWE is important in the context of water resource assessments since it can be used to characterize available water from the seasonal snow cover. This paper presents a new ground-based technique for determining SWE by an acoustic pulse. Ground-based remote-sensing techniques for characterizing snow have been discussed in the literature [2]–[6]. Although based on the idea of sending and receiving acoustic waves into snow [7], our new technique allows for the automated determination of SWE by custom electronic circuits and digital signal processing. This paper will focus on a description of the theory. Field testing will be more extensively described in a companion paper.

Manuscript received September 22, 2008; revised December 1, 2008. First published May 26, 2009; current version published August 28, 2009. This work was supported by the International Polar Year, by the Canadian Foundation for Climate and Atmospheric Sciences through a grant to the IP3 Network, by a National Sciences and Engineering Research Council scholarship, and by the Canada Research Chairs Program.

The authors are with the Centre for Hydrology, University of Saskatchewan, Saskatoon, SK, S7N 5C8, Canada (e-mail: n.kinar@usask.ca; john.pomeroy@usask.ca).

Digital Object Identifier 10.1109/TGRS.2009.2019730

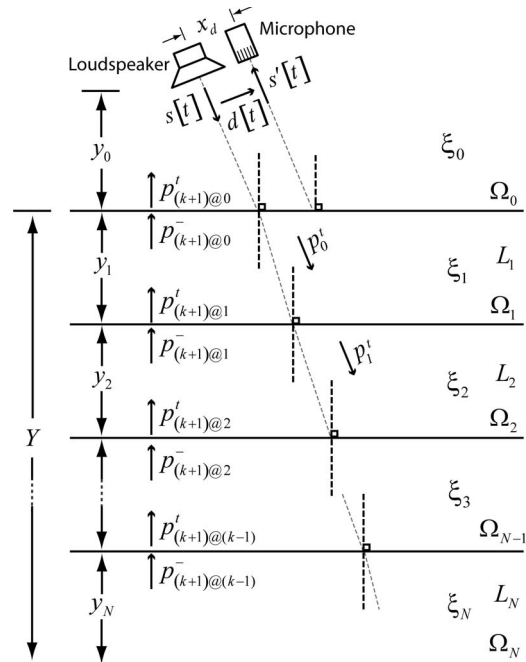


Fig. 1. Diagram of the snowpack showing the snow interfaces.

II. THEORY

A. Snowpack Model

The snowpack model is assumed to be similar to the one described by [7]. A loudspeaker and a microphone are situated at a distance y_0 (in meters) above the surface of a layered snowpack (Fig. 1). The layers represent changes in acoustic impedance, and are not necessarily coincident with stratigraphic layers in the snowpack. The loudspeaker and microphone have a separation distance of x_d (in meters). The loudspeaker produces a sound pressure wave $s[t]$ in the audible frequency range (~ 20 Hz to ~ 20 kHz). The sound pressure wave travels through the air and is coupled into the porous void space of the snowpack. The pulse is reflected from the interfaces $\{\Omega_0, \dots, \Omega_N\}$ between layers $\{L_1, \dots, L_N\}$ in the snowpack due to changes in acoustic impedance. Layer L_0 is considered to be the air layer above the snow surface. An air-coupled direct wave $d[t]$ will also travel between the loudspeaker and the microphone without being reflected from the snowpack. The overall reflection $s'[t]$ of the sound pressure wave from the snowpack is detected by the microphone and then subjected to digital signal processing to obtain the reflection response $r[t]$ of the snowpack. The convolution model incorporating the reflection response $r[t]$ as $s'[t] = s[t] * r[t]$ has been discussed by [7].

B. Snow Interfaces

As a first-order approximation, the interfaces between the layers in the snowpack are considered to produce specular reflections. This is because the scale of the surface roughness features is much smaller than the wavelength of a sound wave in the audible frequency range. However, in a similar fashion to sonar applications, there will be both specular and scattered components of the reflected wave [8]. Fractal techniques are used to model the scattered components by generation of a curve $f[x]$ which has similar properties to a real snow interface [9]. The function used to generate the curve is a band-limited form of the Weierstrass–Mandelbrot function [10], which we recursively define as

$$g[x_0] = \sum_{m=0}^M (D-1)^m \sin(\kappa b_f^m x_0 + \beta_m) \quad (1)$$

$$f[x_0] = \Delta y_{\text{rms}} C g[x_0] \quad (2)$$

$$\Delta y_{\text{rms}} = \left(\frac{1}{N} \sum_{i=0}^{N-1} y_i^2 \right)^{1/2} \quad (3)$$

$$C = \left[\frac{2D(2-D)}{1-(D-1)^{2M}} \right]^{1/2} \quad (4)$$

$$\kappa = \frac{2\pi}{\Lambda}. \quad (5)$$

In (1)–(5), the root-mean-squared (rms) displacement of the interface from a reference level $f[x] = 0$ is Δy_{rms} ; the Hausdorff–Besicovitch (fractal) dimension [11] is given as D ; the total number of harmonic components is M ; the spatial wavenumber is κ (in per meter); the spatial period of displacements in the vertical height of the interface is Λ ; the frequency-scaling parameter is b_f , and the phase-shift at a given harmonic frequency component m is β_m (in radians). The parameters in (1)–(5) are estimated by image analysis of natural snow interfaces [9].

C. Reflection Coefficients and Acoustic Impedance

Owing to continuity of pressure and phase velocity of the sound wave at the snow interfaces, the reflection coefficient Γ_k (dimensionless) of the sound pressure wave can be written in terms of the acoustic impedances ξ_k (in kilograms per square meter second) and ξ_{k+1} (in kilograms per square meter second) of the porous layers L_k and L_{k+1} of the snowpack

$$\Gamma_k = \frac{\xi_{k+1} \cos(\theta_k) - \xi_k \cos(\theta_{k+1})}{\xi_{k+1} \cos(\theta_k) + \xi_k \cos(\theta_{k+1})} \quad (6)$$

where θ_k (in radians) is the angle of incidence of the sound pressure wave in layer L_k at the interface Ω_k , and θ_{k+1} (in radians) is the angle of transmission of the sound pressure wave into layer L_{k+1} . The $\cos(\theta_{k+1})$ term is calculated using: the Snell–Descartes Law (8), which has been written here in an alternate form using: trigonometric identities; and an

expression (7) for the acoustic impedance ξ_k derived by [12] for a porous medium with tortuosity α_k

$$\bar{c}_k = \frac{c_0}{\alpha_k^{1/2}}$$

$$\text{for } \omega > \tilde{\omega} = \frac{2\eta_0}{\rho_0 a^2} \quad (7)$$

$$\bar{c}_{k+1} [\sin(\theta_k)] = \bar{c}_k [\sin(\theta_{k+1})] \quad (8)$$

$$\frac{\alpha_k^{1/2}}{\alpha_{k+1}^{1/2}} \sin(\theta_k) = \sin(\theta_{k+1}) \quad (9)$$

$$\frac{\alpha_k}{\alpha_{k+1}} [\sin(\theta_k)]^2 = 1 - \cos^2(\theta_{k+1}) \quad (10)$$

$$\left\{ 1 - \frac{\alpha_k}{\alpha_{k+1}} [\sin(\theta_k)]^2 \right\}^{1/2} = \cos(\theta_{k+1}). \quad (11)$$

In (7), \bar{c}_k (in meters per second) is the average speed of the sound pressure wave in the pore spaces of the medium; $\omega = 2\pi f$ is the angular frequency of the wave; $\tilde{\omega}$ is a threshold frequency; η_0 (in pascal second) is the dynamic viscosity of the air in the pore spaces of the snow; ρ_0 (in kilograms per meter) is the air density; and a (in meters) is the mean diameter of the pore spaces. The assumption $\omega > \tilde{\omega}$ is valid for sound waves in the audible range propagating through a porous snowpack [9].

A derivation similar to the one shown by (7)–(11) is repeated for the first layer of the snowpack. This is equivalent to setting $\alpha_k = \alpha_0 = 1$ for the air medium. The derivation results in the expression

$$\left\{ 1 - \frac{1}{\alpha_1} [\sin(\theta_0)]^2 \right\}^{1/2} = \cos(\theta_0). \quad (12)$$

The Rayleigh parameter $P_{R,(\Omega,k)}$ (dimensionless) modifies Γ_k to incorporate the scattered components of the reflection [8]

$$\Gamma'_k = \Gamma_k \exp(0.5 P_{R,(\Omega,k)}). \quad (13)$$

The Rayleigh parameter is calculated from the curve $f[x]$ of the fractal snow interface [9]. When the scattered components of the reflection are such that $P_{R,(\Omega,k)} \rightarrow 0$, then it follows that $\Gamma'_k = \Gamma_k$, and the specular component of the reflected wave dominates the reflection.

Calculation of the Rayleigh parameter proceeds in the following fashion. The curve $f[x]$ is generated by recursive application of (1)–(5). The horizontal dimension of the curve $f[x]$ is determined by calculating the footprint or insonified area of the sound wave which has been projected on the snow surface by the loudspeaker. The footprint is calculated by recursively tracking the sound wave as it propagates through the snow and is reflected at the interfaces.

If the loudspeaker and the microphone are situated at nadir, with an angle of incidence of $\theta_k \approx 0$, then the footprint diameter $d_{f,k}$ (m) and area Φ_k (m²) on interface Ω_k of the snowpack is calculated by

$$d_{f,0} = 2y_0 \tan(\varphi/2) \quad (14)$$

$$\Phi_0 = (\pi/4) d_{f,0}^2 \quad (15)$$

$$d_{f,k+1} = d_{f,k} + 2y_{k+1} \tan(\vartheta_{k+1}) \quad (16)$$

$$\Phi_{k+1} = (\pi/4) d_{f,k+1}^2 \quad (17)$$

where y_0 (in meters) is the distance from the sending and receiving transducers to the surface of the snowpack; and φ (in radians) is the aperture angle of the loudspeaker.

If the loudspeaker and microphone are situated at a nonzero angle θ_k to the snow surface (as explicitly depicted in Fig. 1), then the footprint diameter $d_{f,k}^*$ (in meters) and area Φ_k^* (in square meters) are calculated in an alternate fashion

$$d_{f,0}^* = y_0 \left\{ \tan \left(\theta_0 + \frac{\varphi}{2} \right) - \tan \left(\theta_0 - \frac{\varphi}{2} \right) \right\} \quad (18)$$

$$\Phi_0^* = \pi d_{f,0}^* d_{f,0}^* \quad (19)$$

$$\vartheta_{0,A}^* = \theta_0 - \frac{\varphi}{2} \quad (20)$$

$$\vartheta_{0,B}^* = \theta_0 + \frac{\varphi}{2} \quad (21)$$

$$d_{f,k+1}^* = d_{f,k}^* + y_{k+1} \left\{ \tan(\vartheta_{k+1,B}^*) - \tan(\vartheta_{k+1,A}^*) \right\} \quad (22)$$

$$\Phi_{k+1}^* = \pi d_{f,k+1}^* d_{f,k+1}^* \quad (23)$$

D. Propagation of the Pressure Wave

In the absence of any information on the spatial sound radiation pattern of the loudspeaker that produces the sound wave, it is considered to be a point source with an acoustic power P_0 (in watts). This assumption is valid in the far field of the loudspeaker situated above the air–snow interface.

Modeling the propagation of the sound wave by the inverse square law, the pressure p_0^+ (in pascals) of the wave incident on the snow surface interface Ω_1 can be calculated by

$$p_0^+ = \frac{1}{y_0} \left(\frac{\rho_0 c_0 P_0}{2\pi} \right)^{1/2} \quad (24)$$

$$c_0 = (1.4RT^*)^{1/2} \quad (25)$$

$$y_0 = c_0 t_0 \quad (26)$$

where y_0 (m) is the distance from the sending and receiving transducers to the surface of the snowpack, c_0 is the speed of the sound wave in the air medium, and $R = 287 \text{ N} \cdot \text{m} \cdot \text{kg}^{-1} \cdot \text{K}^{-1}$ is the gas constant for air. Calculation of the phase velocity of sound [13] in the air medium c_0 requires an estimate of air temperature T^* (in degrees kelvin). The average phase velocity \bar{c}_k (in meters per second) of the pressure wave in a layer L_k of the snowpack is calculated by (7).

The specular component of the spherical sound wave reflected by the air–snow interface Ω_1 can be modeled as an acoustic “image” [13]. An acoustic source that radiates the reflected wave back toward the receiving transducer is assumed to be situated the same distance y_0 “behind” the interface as the source is situated from the interface. To calculate the power P_1 (in watts) of the point source taken to be the acoustic “image,” the inverse square law is used once again

$$P_1 = \frac{2\pi(2y_0)^2(p_{0,r}^-)^2}{\rho_0 c_0} \quad (27)$$

where $p_{0,r}^-$ (in pascals) is the sound pressure of the first reflection from the snow interface measured at the receiving transducer.

The acoustic power P_1 (in watts) of the reflected image is related to the pressure p_0^- (in pascals) at the snow–air interface by the relationship

$$P_1 = \frac{\Phi_1(p_0^-)^2}{\xi_1} \quad (28)$$

By the definition of the reflection coefficient Γ_1 , (6) and (28) are used to determine the relationship

$$\frac{\xi_{k+1} \cos(\theta_k) - \xi_k \cos(\theta_{k+1})}{\xi_{k+1} \cos(\theta_k) + \xi_k \cos(\theta_{k+1})} \exp(0.5P_{R,(\Omega,k+1)}) - (p_{k+1}^+)^{-1} \left(\frac{P_{k+1} \xi_{k+1}}{A_{k+1}} \right)^{1/2} = 0. \quad (29)$$

The continued propagation of the sound pressure wave in the L_2, \dots, L_N layers of the snowpack is modeled in a recursive fashion. Aside from geometric spreading, attenuation of the wave will occur in this porous medium. Attenuation in the air medium is assumed to be negligible for audible sound frequencies. The attenuation coefficient ψ_k (in per meter) for a layer L_k of dimension y_k (in meters) is calculated from [14]

$$\psi_k = \frac{\partial p_k}{\partial y_k} \frac{1}{2\bar{c}_k \rho_0 c_0} \quad (30)$$

where $\partial p/\partial y$ (in pascals per meter) is the pressure gradient established in the layer L_k . Assuming that the pressure gradient between the interfaces Ω_k and Ω_{k+1} of the snowpack is linear and that the decay rate of the pressure wave in the porous medium is exponential, an expression for the attenuation in the layer is given by [15], which is then used with (30) to yield

$$\psi_k = \frac{p_k^t - p_k^t e^{-\psi_k y_k}}{2y_k \bar{c}_k \rho_0 c_0} \quad (31)$$

$$\text{Log}_e \left(\frac{p_k^t - 2\psi_k y_k \bar{c}_k \rho_0 c_0}{p_k^t} \right) + \psi_k y_k = 0 \quad (32)$$

where y_k (in meters) is the vertical dimension of a layer, the transmitted pressure wave across the interface is p_k^t (in pascals), the phase velocity of the wave in the layer is \bar{c}_k (in meters per second), the density of the air medium is ρ_0 (in kilograms per cubic meter), and the phase velocity of the sound pressure wave in air is c_0 (in meters per second). Because the attenuation coefficient ψ_k is on both sides of (31), Newton iteration is used to find ψ_k from (32), which is a transformed and numerically stable version of this equation.

As the transmitted pressure wave travels in the layer L_k of vertical dimension y_k , loss of wave amplitude will occur due to geometric spreading and attenuation. The incident pressure p_{k+1}^+ (in pascals) of the wave at the Ω_{k+1} interface between the layers L_k and L_{k+1} is given by the inverse square law

$$p_{k+1}^+ = p_k^t \left\{ \left(\frac{\sum_{i=1}^k y_i / \sum_{i=1}^{k+1} y_i}{\sum_{i=1}^{k+1} y_i} \right) - e^{-|\psi_k| y_k} \right\}. \quad (33)$$

Given the pressure $p_{(k+1)@0}^r$ (in pascals) at the receiving transducer reflected from an interface Ω_{k+1} in the snowpack, the source reflection can be used to recursively model

attenuation and geometric spreading of the sound pressure wave through the porous layered medium

$$p_{(k+1)@k}^- = \left(\frac{P_{k+1}\xi_k}{2\pi y_k^2} \right)^{1/2} - e^{-|\psi_k|y_k} \quad (34)$$

$$p_{(k+1)@k}^t = T_{k-1}p_{(k+1)@k}^- \quad (35)$$

$$p_{(k+1)@(k-1)}^- = \frac{p_{(k+1)@k}^t(y_k)}{(y_k + y_{k-1})} - e^{-|\psi_{k-1}|y_{k-1}} \quad (36)$$

$$p_{(k+1)@(k-1)}^t = T_{k-2}p_{(k+1)@(k-1)}^- \quad (37)$$

The procedure recursively continues with (36) and (37) being applied until the first layer L_0 in the snowpack is reached

$$p_{(k+1)@0}^t = T_0p_{(k+1)@0}^- \quad (38)$$

$$p_{(k+1)@0}^r = \frac{p_{(k+1)@0}^t(y_k + L + y_1)}{y_k + L + y_1 + y_0} \quad (39)$$

The nomenclature used in the equations above is used to track the pressures at each of the interfaces in the snowpack. The reflected pressure p_{k+1}^- (in pascals) from the interface Ω_{k+1} becomes the pressure $p_{(k+1)@k}^-$ (in pascals) at the interface Ω_k after propagating backward through the layer L_k . The subscript on the pressure indicates the pressure that is reflected from a layer and the current position of the reflected wave in the layered snowpack. The transmission coefficient T_k for a layer is related to the reflection coefficient by the relationship $T_k = 1 - \Gamma_k$. The vertical dimension of a layer is given by y_k .

The pressure $p_{(k+1)@k}^-$ at the interface Ω_k is determined using back-substitution of (39) to (34). Equation (34) is then solved for P_{k+1} . The pressure P_{k+1} is substituted into (29) so that the porosity ϕ_k of layer L_k can be determined by Newton iteration. The porosity ϕ_k is related to the tortuosity α_k by the Berryman equation [16]

$$\alpha_k = 1 - \gamma \left(1 - \frac{1}{\phi_k} \right) \quad (40)$$

The tortuosity α_k is then used to find the phase velocity \bar{c}_k of the sound pressure wave by (7). In lieu of a better estimate for the dimensionless shape factor γ used in the Berryman expression, the shape factor was estimated to be $\gamma = 0.59$, which is in the middle of the acceptable range $0.5 \leq \gamma \leq 0.67$ of shape factors [9].

Once the porosity ϕ_k and depth y_k of each layer L_k has been determined, the SWE is calculated by the expression [1]

$$\text{SWE} = \frac{1}{N} \left(\sum_{i=0}^N y_i \right) \left(\sum_{i=0}^N \rho_i \right) \quad (41)$$

where $\rho_k = \rho_{\text{ice}}(1 - \phi_k)$, and $\rho_{\text{ice}} = 917 \text{ kg} \cdot \text{m}^{-3}$ is taken to be the nominal density of ice.

III. SIGNAL PRODUCTION AND PROCESSING

The properties of the sent pressure wave $s[t]$ should allow for determination of the reflection response $r[t]$ of the snowpack within a short (~ 1 s) period of time, despite the presence of

environmental sources of noise. It should also allow for $s[t]$ to be adequately reproduced by the loudspeaker, which has a nonlinear frequency response. The signal $s[t]$ was chosen as a maximum-length sequence (MLS) with a length of 7 bits. When applied to determine the impulse response of a system, the signal has these desired properties [17].

The following procedure was used to generate and process the MLS [18]. The MLS is comprised of a set of pseudo-random numbers with length $2^b - 1$, $b \in \mathbb{N}$. The elements in the sequence have only two Boolean states, which are $1 \cup -1$. The positive “1” in this sequence represents a true value, and the negative “-1” represents a false value. The sequence is generated using shift-register methods, which produce a square wave signal with amplitudes $\pm 1|A|$, where A is a scaling factor representing the maximum voltage level sent from the loudspeaker. When the MLS is provided as an input to a linear layered system (such as the snowpack), the correlation of the output signal with the input MLS is the impulse response $r[t]$ of the system. This correlation is calculated by a mathematical procedure known as the fast Hadamard transform (FHT) [18].

When the signal $s'[t]$ is received and digitized by an analog-to-digital converter (ADC), the noise $n[t]$ is removed using a time-warped polynomial filter [19]. The FHT is then applied to the output signal to compute the reflection response $r[t]$.

The $r[t]$ of the layered snowpack found by application of the FHT is similar to the response of the layered snow medium to an impulse created by a pistol being fired in the air above the first snow interface [20]. The noise $n[t]$ in the impulse response is removed using a time-warped polynomial filter [19].

When the signal $r[t]$ is examined as a time-domain plot, various “peaks” can be identified which occur at discrete sampling times [21]. These “peaks” represent reflections from snowpack layers which occur as the incident wave $s[t]$ is reflected from interfaces in the snowpack. Because these are reflections due to changes in acoustic impedance, the reflections are not necessarily coincident with snowpack stratigraphic layers which have developed due to melt or deposition events. By the use of simple kinematics, the travel time of the pressure wave from each of the reflections is determined from the positions of the “peaks” in the time-domain signal.

Because the impulse response signal has the same length as the sampling time of the received signal $s'[t]$, the initial reflections must be separated from the reflections caused by multiple returns. For $r[t]$, this is accomplished by setting a maximum cutoff time t_f beyond which signal processing does not occur [17]. The time t_f is selected from an estimate Y^* of the maximum snow depth over which the P₂-wave propagates. Because the travel times $\{t_0, \dots, t_N\}$ and phase velocities $\{c_0, \dots, c_N\}$ are calculated for each of the reflections from the acoustic model [7], the cumulative propagation depth of the pressure wave traveling through the pore spaces of the snowpack is calculated for each recursive application of the model. The signal processing algorithm stops at the time when the cumulative propagation depth exceeds the estimated depth Y^* (in meters). Unwanted reflections in the truncated signal contribute to the experimental error of the acoustic reflectometry technique. Fig. 2 is an example of the truncated signal. The amplitude has been normalized with respect to the highest voltage digitized by the ADC.

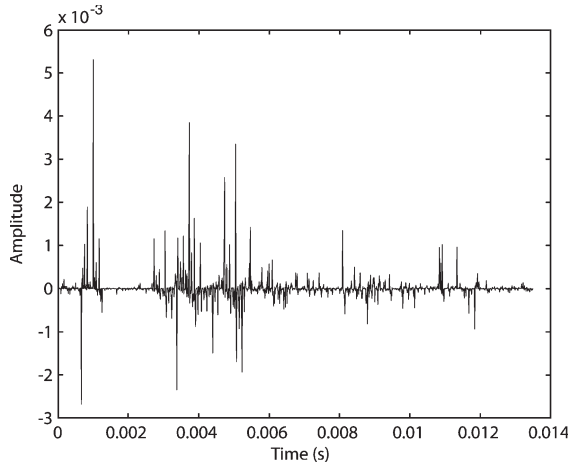


Fig. 2. Truncated reflection response of the snowpack exhibiting “peaks.”

The “peaks” in the FHS-transformed signal are identified by an algorithm given by [22]. Linear piecewise curve fitting is used to find the slopes of lines joining successive elements on a plot of the signal sequence. The slopes are matched to patterns in a predefined lookup table, which creates a “string” comprised of the patterns. The “string” is then parsed according to a Backus–Naur context-free grammar, which enables the detection of a “peak.” Further details on the implementation of this algorithm are given in [22].

The sound pressure waves $p_{(k+1)\text{@}0}^r$ correspond to the “peaks” $\{\Xi_0, \dots, \Xi_N\}$ in the sequence found by the peak-detector algorithm. The relationship between the voltage output E_k of the microphone corresponding to the Ξ_k peak in the sequence and the pressure (in pascals) of the received sound wave is given by [13]

$$p_{(k+1)\text{@}0}^r = E_k(10^{-L_s/20}) \quad (42)$$

where L_s is the microphone sensitivity given in units of decibels-volts per microbar. Equation (42) is used to find the pressure of each “peak” identified by the peak detector.

The contribution of the air-coupled direct wave $d[t]$ which travels between the loudspeaker and the microphone is difficult to predict because the sensing system consists of only one receiving microphone. Another transducer could be positioned between the loudspeaker and the microphone, but sampling of the pressure wave in this fashion requires an additional electronic circuit and also increases the processing time. Moreover, the presence of another transducer may affect the spatial sound pressure distribution of the direct air-coupled wave, and the estimation of $d[t]$ would be inaccurate. To remove $d[t]$, the contribution of the air-coupled wave to $s'[t]$ is considered to be similar to crosstalk between two wires. Crosstalk occurs in electronics when a signal produced in one channel of a data system leaks over to another channel, creating an unwanted signal. Removal of $d[t]$ utilizes a crosstalk minimization algorithm presented by [23]. The minimization proceeds within a moving window. The width of the moving window was chosen to be 512 samples in the signal $s'[t]$. The moving window reduces the computation time of the minimization algorithm, and also compensates for temporal changes in the noise level.

Once a δ coefficient has been found by the minimization algorithm, the air-coupled wave is calculated as $d[t] = \delta s[t]$ and subtracted from $s'[t]$.

IV. MATERIALS AND METHODS

A. Prototype Circuits

Two prototype electronic circuits were constructed to send the sound pressure wave into the snowpack and to conduct digital signal processing on the reflected wave received by the microphone. The two circuits incorporated 32-bit digital signal processors (DSPs) running at a nominal speed of 210 million instructions per second. The loudspeaker and the microphone were mounted on the side of an electronic circuit enclosure box. The positions of the microphone and the loudspeaker had the same geometry, as shown in Fig. 1. The separation distance between the loudspeaker and the microphone was 4.5 cm. A trigger grip fastened to the underside of the enclosure box allowed a snow surveyor to hold the loudspeaker and microphone above the snow surface. A push-button fastened on the trigger grip allowed for the snow surveyor to generate a microcontroller interrupt, which instructed the system to send a 1-s sound pulse from the loudspeaker. The reflection from the snowpack was digitized and transferred to volatile (SDRAM) memory by the DSP.

Because the DSP processors had an integrated memory management unit, it was possible to natively run a version of the Linux kernel on this embedded system. The high speed of the DSPs and the embedded operating system permitted the data to be completely processed in the field, without being offloaded to an external datalogger. A digital readout permitted the acoustic estimates of SWE to be presented to the snow surveyor within an average wait-time of 15 s after the initial press of the button.

Although the systems consumed approximately 1.25 A of current at peak operation, it was possible to power the system continuously for 2.5 h with a Lithium-ion battery pack rated at 3000 mA · h. Due to the large amount of current consumed by the DSP and processing circuitry, it was only possible to collect a limited number of samples at the two field sites. The architecture of the embedded systems is described in more detail by [21].

B. Field Locations

The prototypes were tested at two field sites. The first prototype was tested during the late winter of 2007 in Wolf Creek Research Basin, near Whitehorse, YT, Canada, whereas the second device was tested during the winter of 2008 at field locations in the Rocky Mountains of Alberta, Canada. Gravimetric sampling techniques [1] involving snow pits and an ESC30 sampler [24] were used to determine estimates of SWE for comparison.

The snow at these two field sites represent observations at environmental locations characteristic of cold, thin Arctic snow with low shrub; cold boreal forest; and deep, dense and sometimes wet mountain snow. Observations were taken over a range of 10° latitude and 20° longitude. This is a test backed by other preliminary studies conducted in Saskatchewan and

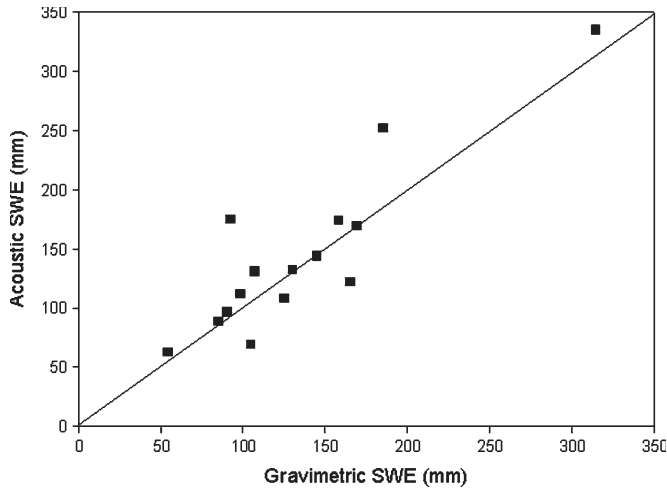


Fig. 3. Comparing the gravimetric and acoustic estimates of SWE for the Yukon sites.

British Columbia which have demonstrated that it is possible to determine SWE by an acoustic wave [7].

V. RESULTS AND ANALYSIS

To compare the accuracy of the acoustic technique to gravimetric sampling and to examine the differences between the Yukon and Rocky Mountain sites, the correlation coefficients between the acoustic and gravimetric data sets were calculated. For sites where two types of gravimetric measurements were taken (snow pit and ESC30), the snow pit measurements were used in lieu of the ESC30 measurements. This is because the snow pit measurements are considered more accurate than the ESC30 measurements [21]. The slope of the best fit lines through the data points and the root mean squared error (rmse) was also calculated.

The correlation coefficient between the gravimetric and acoustic SWE data sets collected at the Yukon sites was $R^2 = 0.79$ (Fig. 3, slope = 1.028, rmse = 33 mm; standard error = 0.188) from 15 samples. Alternately, the correlation coefficient between the gravimetric and acoustic SWE data sets collected at the Rocky Mountain sites was $R^2 = 0.95$ (Fig. 4, slope = 1.016, rmse = 32 mm; standard error = 0.134) from 33 samples. These results show that the rmse in determining SWE is approximately the same at two distinct geographic sites, demonstrating that the method is robust for a wide variety of environmental circumstances. The strength of the linear relationship between the gravimetric and acoustic SWE estimates is lower for the Yukon sites as compared to the Rocky Mountain sites. This is due to the presence of ice layers, wind crusts, and vegetation which causes acoustic scattering of the wave, and this increases the variability in the acoustic estimates of SWE. The correlation coefficient at the Rocky Mountain sites is higher than the correlation coefficient at the Yukon sites due to the greater number of samples and a more linear relationship due to less acoustic scattering of the sound wave.

The effects of vegetation and rough surfaces on the acoustic predictions of SWE was determined by selecting the acoustic and gravimetric SWE data for sample points which were known to be characteristic of vegetation or surface roughness. Although there might have been other sample points which

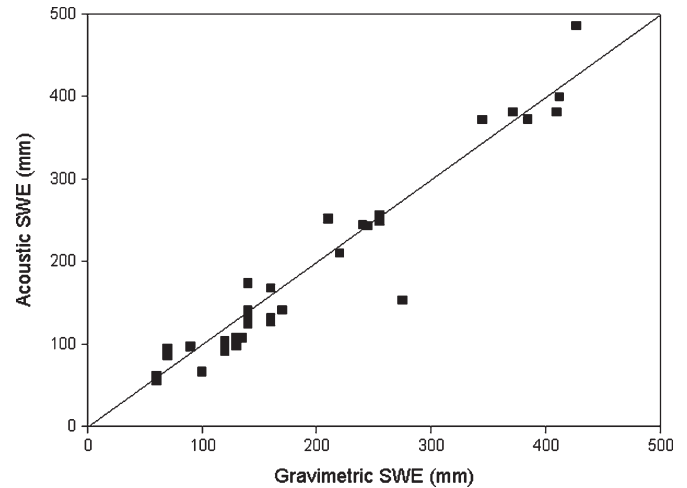


Fig. 4. Comparing the gravimetric and acoustic estimates of SWE for the Rocky Mountain sites.

were affected by these characteristics, only those data points which were documented in our field observations notebooks as having these attributes were considered.

The correlation coefficient between the gravimetric and acoustic SWE data sets selected to be representative of vegetation effects was $R^2 = 0.096$ (slope = 0.218, rmse = 42 mm; standard error = 0.261) from six samples. The correlation coefficient between the gravimetric and acoustic SWE data sets selected to be representative of rough surfaces was $R^2 = 0.84$ (slope = 1.29, rmse = 34.7 mm; standard error = 0.234) from six samples.

The results of this comparison demonstrate that acoustic scattering due to vegetation is a significant limiting factor of the acoustic SWE technique. This is due to scattering of sound by vegetation under the snow. The diffuse reflection of the sound wave due to the presence of rough surfaces can give results that have an adequate linear relationship and an acceptably small error.

VI. CONCLUSION

Experiments at a mixture of forested and open sites in two geographically distinct regions over two winter field seasons demonstrated that an acoustic MLS sequence and a novel pressure-tracking algorithm can determine SWE with accuracy comparable to the differences between gravimetric sampling by snow pit and ESC30 snow tube. The snow tested using this technique ranged between SWE values of 50 to 500 mm. This indicates that the technique is applicable to snow with SWE values in this range. Further research is required to determine the full range of environmental conditions over which the acoustic technique can be applied, and to determine the effects of snow wetness on the acoustic model.

Further research is also required to mathematically model the interactions of the sound wave with ice layers and vegetation. Prediction of sound wave scattering by buried vegetation may help to provide insights into mitigating this effect and improving the acoustic estimates of SWE.

The use of a fixed shape factor $\gamma = 0.59$ allows for SWE to be adequately predicted by an acoustic wave at two field sites

by averaging the estimates of density calculated from each of the layers. This suggests that this value is adequate for most operational deployments of the acoustic SWE gauge, but setting shape factors to local conditions may improve the accuracy with which SWE is determined by an acoustic wave.

This paper demonstrates that SWE can be determined using acoustic waves by an automated procedure and custom electronic circuits. It is possible that this technique may eventually prove to be valuable to snow surveyors, who currently have to extract snow samples from the snowpack to determine SWE. The use of a noninvasive method has the potential to revolutionize snow surveying and permit snow samples to be taken much more quickly than with a snow tube or snow pit. This allows for snow surveyors to perform their task quickly and allows for a greater number of sampling points to be collected.

A potential barrier to the immediate adoption of this technique is the amount of power consumed by the experimental systems. There is a need to design power-efficient and portable systems which are able to continuously take measurements of SWE in cold environments.

Other potential applications for the acoustic SWE gauge include automated determination of SWE at a fixed site in remote locations and the examination of high-resolution temporal changes in the snowpack. Further research is planned to verify the conclusions presented in this paper and assess the feasibility of these other novel applications of the technology, particularly for use in studies of snowpack stratigraphy.

ACKNOWLEDGMENT

The authors would like to thank W. Helgason, P. Dornes (University of Saskatchewan), and R. Janowicz (Yukon Environment) for logistical assistance at the Wolf Creek sites, as well as A. Sabourin (L'Ecole Polytechnique Paris, France), R. Essery (University of Edinburgh, U.K.), and the University of Calgary Biogeoscience Institute for assistance with the field campaign conducted in the Rocky Mountains. The authors would also like to thank the two anonymous reviewers, whose comments have greatly improved this paper.

REFERENCES

- [1] J. W. Pomeroy and D. M. Gray, *Snowcover: Accumulation, Relocation, and Management*. Saskatoon, SK, Canada: Nat. Water Res. Inst., 1995, pp. 1–20.
 - [2] M. Parde, K. Goita, A. Royer, and F. Vachon, “Boreal forest transmissivity in the microwave domain using ground-based measurements,” *IEEE Geosci. Remote Sens. Lett.*, vol. 2, no. 2, pp. 169–171, Apr. 2005.
 - [3] A. A. Kokhanovsky, T. Aoki, A. Hachikubo, M. Hori, and E. P. Zege, “Reflective properties of natural snow: Approximate asymptotic theory versus in situ measurements,” *IEEE Trans. Geosci. Remote Sens.*, vol. 43, no. 7, pp. 1529–1535, Jul. 2005.
 - [4] J. I. Peltoniemi, S. Kaasalainen, J. Naranen, L. Matikainen, and J. Piironen, “Measurement of directional and spectral signatures of light reflectance by snow,” *IEEE Trans. Geosci. Remote Sens.*, vol. 43, no. 10, pp. 2294–2304, Oct. 2005.
 - [5] G. Luzi, M. Pieraccini, D. Mecatti, L. Noferini, G. Macaluso, A. Tamburini, and C. Atzeni, “Monitoring of an Alpine glacier by means of ground-based SAR interferometry,” *IEEE Geosci. Remote Sens. Lett.*, vol. 4, no. 3, pp. 495–499, Jul. 2007.
 - [6] G. Luzi, M. Pieraccini, L. Noferini, D. Mecatti, G. Macaluso, C. Atzeni, P. Joerg, and R. Sailer, “Ground-based microwave interferometric measurements over a snow covered slope: An experimental data collection in Tyrol (Austria),” in *Proc. IEEE IGARSS*, 2007, pp. 1452–1455.
 - [7] N. J. Kinar and J. W. Pomeroy, “Determining snow water equivalent by acoustic sounding,” *Hydrol. Process.*, vol. 21, no. 19, pp. 2623–2640, Sep. 2007.
 - [8] X. Lurton, *An Introduction to Underwater Acoustics: Principles and Applications*. New York: Springer-Verlag, 2002, pp. 61–102.
 - [9] N. J. Kinar and J. W. Pomeroy, “Operational techniques for determining SWE by sound propagation through snow: I. General theory,” in *Proc. Eastern Snow Conf.*, 2008, vol. 65, pp. 309–323.
 - [10] J. E. Summers, R. J. Soukup, and R. F. Gragg, “Characterization and fabrication of synthetic rough surfaces for acoustical scale-model experiments,” Naval Res. Lab., Washington DC, Naval Res. Lab. Rep. NRL/MR-MM/7140-05-8871, 2005.
 - [11] J. Szulga, “Hausdorff dimension of Weierstrass–Mandelbrot process,” *Stat. Probab. Lett.*, vol. 56, no. 3, pp. 301–307, 2002.
 - [12] O. Umnova, K. Attenborough, H. C. Shin, and A. Cummings, “Deduction of tortuosity and porosity from acoustic reflection and transmission measurements on thick samples of rigid-porous materials,” *Appl. Acoust.*, vol. 66, no. 6, pp. 607–624, Jun. 2005.
 - [13] D. R. Raichel, *The Science and Applications of Acoustics*, 2nd ed. New York: Springer-Verlag, 2006, pp. 16–176.
 - [14] E. Meyer and E.-G. Neumann, *Physical and Applied Acoustics: An Introduction*. New York: Academic, 1972, pp. 13–17.
 - [15] H. Kuttruff, *Acoustics: An Introduction*. New York: Taylor & Francis, 2007, p. 56.
 - [16] J. G. Berryman, “Confirmation of Biot’s theory,” *Appl. Phys. Lett.*, vol. 37, no. 4, pp. 382–384, Aug. 1980.
 - [17] D. D. Rife and J. Vanderkooy, “Transfer-function measurement with maximum-length sequences,” *J. Audio Eng. Soc.*, vol. 37, no. 6, pp. 419–444, Jun. 1989.
 - [18] J. Borish and J. B. Angell, “An efficient algorithm for measuring the impulse response using pseudorandom noise,” *J. Audio Eng. Soc.*, vol. 31, no. 7/8, pp. 478–488, Aug. 1983.
 - [19] W. Philips, “Adaptive noise removal from biomedical signals using warped polynomials,” *IEEE Trans. Biomed. Eng.*, vol. 43, no. 5, pp. 480–492, Jul. 1996.
 - [20] D. G. Albert, “A comparison between wave propagation in water-saturated and air-saturated porous materials,” *J. Appl. Phys.*, vol. 73, no. 1, pp. 28–36, Jan. 1993.
 - [21] N. J. Kinar and J. W. Pomeroy, “Operational techniques for determining SWE by sound propagation through snow: II. Instrumentation and testing,” in *Proc. Eastern Snow Conf.*, 2008, vol. 65, pp. 19–33.
 - [22] S. L. Horowitz, “A syntactic algorithm for peak detection in waveforms with applications to cardiology,” *Commun. ACM*, vol. 18, no. 5, pp. 281–285, May 1975.
 - [23] J. F. Claerbout, *Earth Soundings Analysis: Processing Versus Inversion*. Boston, MA: Blackwell Sci. Publications, 1992.
 - [24] B. E. Goodison, H. L. Ferguson, and G. A. McKay, “Measurement and data analysis,” in *Handbook of Snow: Principles, Processes, Management, and Use*, D. M. Gray and D. H. Male, Eds. Toronto, ON, Canada: Pergamon, 1981, pp. 191–274.
- Nicholas J. Kinar**, photograph and biography not available at the time of publication.
- John W. Pomeroy**, photograph and biography not available at the time of publication.